Central European Journal of Energetic Materials
ISSN 1733-7178; e-ISSN 2353-1843

Cent. Eur. J. Energ. Mater. 2019, *16*(4): 504-519; DOI 10.22211/cejem/115251
Article is available in PDF-format, in colour, at:
http://www.wydawnictwa.ipo.waw.pl/cejem/Vol-16-Number-4-2019/CEJEM_00976.pdf

Research paper

Numerical Simulation of the Deflagration to Detonation Transition in Granular High-Energy Solid Propellants

Fei Zhen, Liqiong Wang*, Zhuoqun Wang

State Key Laboratory of Explosion Science and Technology, Beijing Institute of Technology, 100081 Beijing, China
**E-mail:* wlq2018@sina.com

Abstract: This paper describes a one-dimensional code developed for analyzing the two-phase deflagration to detonation transition (DDT) phenomenon in granular high-energy solid propellants. The deflagration to detonation transition model was established based on a one-dimensional two-phase reactive flow model involving basic flow conservation equations and constitutive relations. The whole system was solved using a high resolution 5th-order WENO (Weighted Essentially Non-Oscillatory) scheme for spatial discretization, coupled with a 3rd-order TVD Runge-Kutta method for time discretization, to improve the accuracy and prevent excessive dispersion. An inert two-phase shock tube problem was carried out to access the developed code. The DDT process of high-energy solid propellants was simulated and the parameters of detonation pressure, run distance to detonation and time to detonation were calculated. The results show that for a solid propellant bed with solid volume fraction 0.65, the run distance to detonation was about 120 mm, the detonation induced time was 28 μs, and the detonation pressure was 18 GPa. In addition, the effects of solid volume fraction (φ_s) and pressure exponent (n) on the deflagration to detonation transition were also investigated. The numerical results for the DDT phenomenon are in good agreement with experimental results available in the literature.

Keywords: deflagration to detonation transition, two-phase reactive flow model, WENO, solid volume fraction, pressure exponent

1 Introduction

Study on the deflagration to detonation transition (DDT), which is one of the important characteristics of energetic materials, has been conducted for many decades, in both industrial and military studies. This phenomenon is a complex solid combustion problem and is influenced by a variety of factors. DDT has been physically investigated by typical Macek's tube experiments [1, 2] and piston-ignited DDT experiments [3-5] in order to obtain a mechanistic description of the phenomenon. Bernecker [6] reviewed the DDT process and the variables that influence it in porous high-energy propellants. Recently, McAfee [7] summarized many of the physical observations of the DDT process and systematically elucidated the DDT mechanism for energetic materials with different densities, defining the major types of DDT. However, it is difficult to describe the transition to detonation accurately and quantitatively because of the complex nature of the DDT process. Therefore, the present paper attempts to study the DDT process of a high-energy solid propellant by numerical simulation, in order to provide the basis for the safe production, storage and use of propellants.

At present, three main reactive flow models, varying from single phase to three phases, have been developed to simulate the deflagration to detonation transition in granular energetic materials [8-11]. Two-phase flow models, including the Baer-Nunziato (BN) model proposed by Baer, Nunziato *et al.* [12, 13] and the Powers-Stewart-Krier (PSK) model proposed by Powers *et al.* [14], are widely used to numerically simulate the DDT process of an energetic material. The two-phase flow models are based on the evolution of gases and solids. The BN model and the PSK model are two effective models for simulating the DDT process of the energetic materials. The BN model can be used to describe one-dimensional two-phase reactive flow in the granular bed, and the PSK model can be used to predict the compaction wave in response to a piston-driven boundary condition.

For further understanding the mechanism of the DDT for granular high-energy solid propellants, a one-dimensional two-phase reactive flow model based on the BN model was established for simulating the DDT process. A high precision solution method with a 5th-order WENO scheme for spatial discretization and a 3rd-order TVD Runge-Kutta method for time discretization was applied for numerically predicting the DDT process of granular high-energy solid propellants. The effects of the solid volume fraction and the pressure exponent on the DDT of granular high-energy solid propellants were studied.

2 Basic Model and Numerical Method

The model used in this study is based on two-phase reactive flow theory. It is assumed that each phase is continuous and occupies a certain volume. The conservation equations of the gas and solid phases include conservation equations considering the mass exchange and the transfer of energy and momentum between the gas and solid phases. In addition, the state equation of the gas phase was described by Noble-Abel equations, and the state equation of the solid phase was described by Helmholtz equations. The partial differential equations describing the DDT process in the granular high-energy solid propellant bed are as follows.

The basic equations for one-dimensional two-phase flow could be written as:

$$\frac{\partial \varphi_g \rho_g}{\partial t} + \frac{\partial \varphi_g \rho_g u_g}{\partial x} = \Gamma_g \tag{1}$$

$$\frac{\partial \varphi_s \rho_s}{\partial t} + \frac{\partial \varphi_s \rho_s u_s}{\partial x} = -\Gamma_g \tag{2}$$

$$\frac{\partial \varphi_g \rho_g u_g}{\partial t} + \frac{\partial \left(\varphi_g \rho_g u_g^2 + \varphi_g p_g\right)}{\partial x} = \Gamma_g u_s - D \tag{3}$$

$$\frac{\partial \varphi_s \rho_s u_s}{\partial t} + \frac{\partial \left(\varphi_s \rho_s u_s^2 + \varphi_s p_s\right)}{\partial x} = -\Gamma_g u_s + D \tag{4}$$

$$\frac{\partial \varphi_g \rho_g \left(e_g + u_g^2/2\right)}{\partial t} + \frac{\partial \left[\varphi_g \rho_g u_g (e_g + u_g^2/2 + p_g/\rho_g)\right]}{\partial x} = \Gamma_g \left(e_s + u_s^2/2\right) - D u_s - \overset{g}{Q} \tag{5}$$

$$\frac{\partial \varphi_s \rho_s \left(e_s + u_s^2/2\right)}{\partial t} + \frac{\partial \left[\varphi_s \rho_s u_s (e_s + u_s^2/2 + p_s/\rho_s)\right]}{\partial x} = -\Gamma_g \left(e_s + u_s^2/2\right) + D u_s + \overset{g}{Q} \tag{6}$$

where φ, ρ, u and e are the volume fraction, density, velocity and internal energy, respectively; subscripts g and s represent the properties of the gas and solid phase, respectively; Γ_g is the gas generation rate per unit volume; D and $\overset{g}{Q}$ are the interphase drag interaction term and the interphase heat transfer interaction term, respectively. The equations for the interphase terms are expressed in Equations 7-9:

$$\Gamma_{\mathrm{g}} = \frac{3}{r_s}\varphi_s \rho_s \left(a p_{\mathrm{g}}^{n}\right) \tag{7}$$

$$D = \frac{\mu_{\mathrm{g}}}{\left(4 a p_g^{n}\right)^2}\left(u_{\mathrm{g}} - u_s\right) f_{s\mathrm{g}} \tag{8}$$

$$\overset{\mathrm{g}}{Q} = \frac{3}{r_s}\varphi_s h_{s\mathrm{g}} \left(T_{\mathrm{g}} - T_s\right) \tag{9}$$

where r_s is the particle radius; μ_g indicates the gas viscosity coefficient; a and n are the burning rate coefficient and the pressure exponent, respectively, which can be obtained from strand burning rate data [16]. f_{sg} and h_{sg} are the mean interphase drag interaction coefficient and the interphase heat transfer interaction coefficient, respectively. These are expressed in Equations 10 and 11:

$$f_{s\mathrm{g}} = \left(\frac{\varphi_s}{\varphi_{\mathrm{g}}}\right)^2 \left[276 + 5\left(\frac{Re}{\varphi_s}\right)^{0.87}\right] \tag{10}$$

$$h_{s\mathrm{g}} = 0.375 \frac{\kappa_{\mathrm{g}}}{r_s} Re^{0.7} Pr^{0.33} \tag{11}$$

where, κ_g denotes the thermal conductivity of the gas; *Re* and *Pr* denote Reynolds and Prandtl numbers, respectively.

The state equation of the gas phase can be expressed by Equations 12 and 13, and the state equation of the solid phase can be expressed by Equations 14 and 15:

$$p_{\mathrm{g}} = \rho_{\mathrm{g}} R_{\mathrm{g}} T_{\mathrm{g}} \left(1 + \eta \rho_{\mathrm{g}}\right) \tag{12}$$

$$de_{\mathrm{g}} = c_{\mathrm{vg}} dT_{\mathrm{g}} \tag{13}$$

$$p_s = c_{vs}\left(T_s - T_{s0}\right)\Gamma_s \rho_s + \frac{K_{\mathrm{T}}}{N}\left[\left(\frac{\rho_s}{\rho_{s0}}\right)^{N} - 1\right] \tag{14}$$

$$e_s = c_{vs}\left[\left(T_s - T_{s0}\right) - T_{s0}\Gamma_s\rho_s\left(\frac{1}{\rho_{s0}} - \frac{1}{\rho_s}\right)\right] + \frac{K_T}{\rho_{s0}N\left(N-1\right)}\left[\left(\frac{\rho_s}{\rho_{s0}}\right)^N - \left(N-1\right)\left(1 - \frac{\rho_{s0}}{\rho_s}\right) - 1\right] \quad (15)$$

where R_g and η are constants of the state equation of the gas phase; K_T and N denote the isothermal bulk modulus and compression constant in the state equation of the solid phase, respectively; c_{vg} and c_{vs} are constants for the volume specific heats for the gas and solid phases, respectively. Subscript 0 is used to define the initial values.

The interphase force balance of the solid is modelled by Equations 16-20 from Carroll and Holt [15]. Furthermore it is assumed that pore collapse occurs in three phases, elastic phase, elastic-plastic phase and plastic phase. The equilibrated stress (p^e) of the elastic phase ($\alpha_0 \geq \alpha > \alpha_1$), the elastic-plastic phase ($\alpha_1 \geq \alpha > \alpha_2$) and the plastic phase ($\alpha_2 \geq \alpha > 1$) are expressed in Equations 16-18, respectively:

$$p^e = \frac{4G'\left(\alpha_0 - \alpha\right)}{3\alpha\left(\alpha - 1\right)} \quad (16)$$

$$p^e = \frac{2}{3}Y\left[1 - \frac{2G'}{Y\alpha}\left(\alpha_0 - \alpha\right) + \ln\left(\frac{2G'\left(\alpha_0 - \alpha\right)}{Y\left(\alpha - 1\right)}\right)\right] \quad (17)$$

$$p^e = \frac{2}{3}Y\ln\frac{\alpha}{\alpha - 1} \quad (18)$$

where parameter α is the void porosity and is equal to $1/\varphi_s$; Y and G' are the yield strength and shear modulus, respectively. α_1 and α_2 are defined in Equations 19 and 20:

$$\alpha_1 = \frac{2G'\alpha_0 + Y}{2G' + Y} \quad (19)$$

$$\alpha_2 = \frac{2G'\alpha_0}{2G' + Y} \quad (20)$$

The balance of the static force is expressed as Equation 21:

$$p_s = p_g + p^e \quad (21)$$

The mixture saturation condition is given by Equation 22:

$$\varphi_g + \varphi_s = 1 \tag{22}$$

All model constants used in the calculation are listed in Table 1 [12, 17].

Table 1. Model constants

Parameter	Unit	Value
a	[m/(s·Pa)]	$2.9 \cdot 10^{-9}$
N	–	0.9
η	[m^3/kg]	$1.1 \cdot 10^{-3}$
c_{vg}	[J/(kg·K)]	$1.77 \cdot 10^3$
$\Gamma_s \rho_s$	[kg/m^3]	$2.05 \cdot 10^3$
K_T	[Pa]	$1.2 \cdot 10^9$
N	–	10.3
c_{vs}	[J/(kg·K)]	$1.5 \cdot 10^3$
Y	[Pa]	$5.9 \cdot 10^6$
G'	[Pa]	$6.7 \cdot 10^7$

As the governing equations are highly coupled and the DDT process is inherently unsteady, a numerical integration method is required. A one-dimensional code was developed in this study, with a high resolution method using a 5th-order WENO scheme [18, 19] for spatial discretization, coupled with a 3rd-order TVD Runge-Kutta method for time discretization.

3 Results and Discussion

3.1 Validation of One-dimensional Code

To verify the stability and accuracy of the one-dimensional code developed in this study, the commonly known inert two-phase shock tube problem [20] was solved first. For an inert two-phase shock tube problem, a one-dimensional tube is separated into two distinct regions by a diaphragm. The initial condition for the two regions at $t = 0$ is expressed by Equation 23 and the state equations of the gas and solid phases are expressed by Equations 24 and 25, respectively.

$$(\rho_i, u_i, p_i) = \begin{cases} (10,0,10) & 0 < x < 5 \\ (1,0,1) & 5 < x < 10 \end{cases} \tag{23}$$

$$p_i = \rho_i R_i T_i \tag{24}$$

$$e_i = c_{vi} T_i \tag{25}$$

where subscript i denotes the gas or solid phase. In these calculations, 1000 cells with reflection boundary conditions were considered. Specific heat capacities c_{vg} and c_{vs} for gas and solid in the equation of state are equal to 718 and 239 J/(kg·K), respectively. R_g is equal to R_s as 287 J/(kg·K) [21]. The computed results using the code developed in this study were compared with the exact solution [22].

The simulated results are shown in Figure 1. The results by the WENO Runge-Kutta method have a better accuracy compared with those using other methods at the position of shock-discontinuity and are in good agreement with the exact solutions. The pressure deviation of several methods was about 0% at the continuity, and the maximum deviation by the WENO Runge-Kutta method was 0.6% lower than that of other numerical methods at the discontinuity. Numerical simulation for grid independency with 200, 800 and 1000 grid-points resolution was also carried out. The simulated results of the gas phase pressure from a close-up view are shown in Figure 2. It may be seen that with an increase in the grid resolution, the shock-discontinuity appeared as convergent behaviour. At the discontinuity $x = 2.5$, the deviation of 1000 grid-points resolution was lower than 1.0%. So using $N = 1000$ for the grid independency point for the calculations was accepted. Based on the results from different numerical methods and under different grid resolutions, a high resolution method using the WENO scheme coupled with the TVD Runge-Kutta method with 1000 grid-points resolution was performed for the numerical simulation of the DDT.

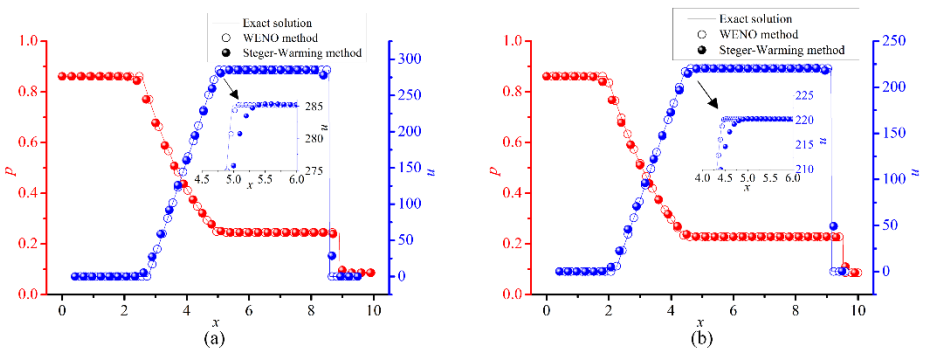

Figure 1. Pressure and velocity comparisons of the exact and numerical solutions for the inert two-phase shock tube simulation at 7 ms: (a) gas phase, (b) solid phase

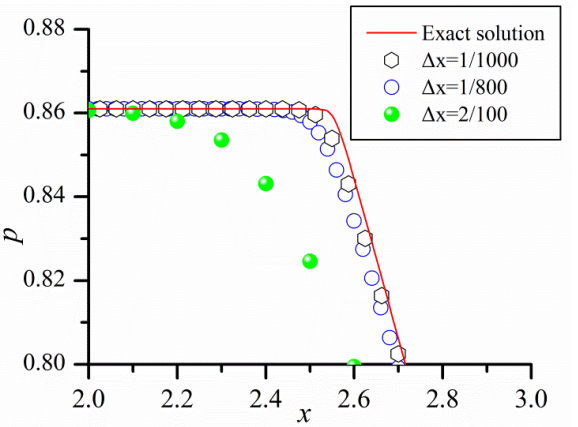

Figure 2. $p-x$ curves of the gas phase under different grid resolutions in close-up

3.2 Effect of solid volume fraction on DDT

The DDT process of the granular drug bed with a grain size of 200 μm for high-energy solid propellants was simulated. The initial solid phase density is $\rho_{s0} = \varphi_{s0} \cdot \rho_{pro}$. ρ_{pro} is the maximum theoretical density (TMD) for the solid propellant, 1860 kg/m^3. The solid volume fraction φ_{s0} (the porosity ratio of the solid propellant) of the granular drug bed is 0.65. The computational domain with 20 mm ignition zone and 400 mm granular drug bed was discretized. Furthermore it was assumed that the DDT process started from the ignition zone, in which the gas volume fraction is 1, and the density and specific internal energy phase are 80 kg/m^3 and $2.4 \cdot 10^6$ J/kg, respectively. Based on the above data, the temperature and pressure were calculated by the state equation. In addition, the temperature of the granular drug bed was assumed to be equal to the ambient temperature, *i.e.* 300 K. The critical ignition temperature was set to 450 K. The boundary was assumed to be an adiabatic rigid interface.

Figure 3 shows the pressure-distance profiles of the gas phase at different times. Many characteristics of the DDT process could be observed. It may be seen from the results that the pressure changes can be roughly divided into three stages. At the beginning of the combustion, the maximum pressure was located at the ignition, and there was no peak pressure. Then, with the increase in gaseous products and pressure, the pressure distribution became more and more obvious. A sharp increase was observed during the process from an initial pressure 0.1 MPa to about 18 GPa after initiation. The compression wave formed and grew gradually. After steady detonation, the pressure increased slightly, but the change was not obvious. The duration of deflagration was about 28 μs and the spatial location of the transition was about 120 mm. The calculated

particle velocity of the gas was 2.04 km/s at the C-J state. After combustion changed into detonation, a steady compression wave propagated through the domain, and the pressure of the gas phase was maintained at about 18 GPa. The distance-time diagrams of the flame front given by numerical simulation and experiment may be seen in Figure 4. The DDT process underwent ignition, deflagration and detonation, in which the deflagration only takes a short time. The predicted results for the position and time of the ignition front are in good agreement with experimental data from Price and Berneck [23].

Figure 5 shows the evolution of the solid volume fraction during the DDT process, as well as the flame spreading and granular bed compression phenomena in a metal tube. In the process of DDT, there are two zones, a combustion zone and a compression zone, which have important influences on the transition to detonation. In the combustion zone A-B, flame propagation decreases the solid volume fraction by consuming granular solid propellant. The generated high temperature and high pressure gaseous products penetrate through the porous structure of the granular propellant bed, and suppress the granular bed, resulting in an increase in the solid volume fraction and formation of a compressed bed B-C. From the simulation results, the combustion process and the compression process were observed in the deflagration stage as well as the detonation stage. In the deflagration stage $t = 8$ μs, the thickness of the combustion zone D_{AB} was 10.9 mm, which is larger than the thickness of the compressed bed D_{BC} 4.6 mm. In the detonation stage $t = 42$ μs, the two thicknesses D_{AB} and D_{BC} were 6.3 and 1.6 mm, respectively, which are smaller than those in the deflagration stage.

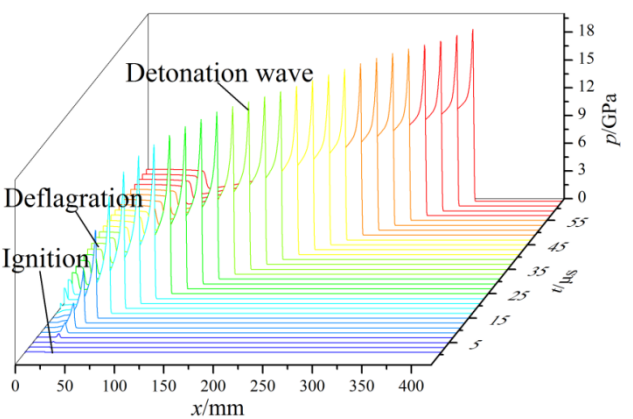

Figure 3. p = f(x) relation of the gas phase at different times during the DDT process

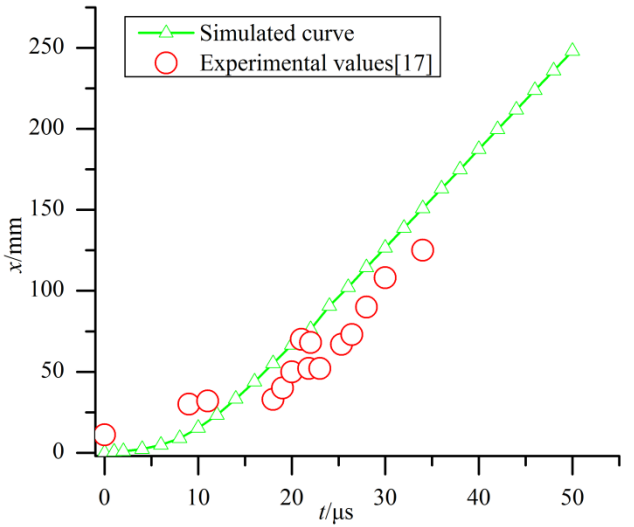

Figure 4. Comparison of $x = f(t)$ relation of flame front by simulation and by experiment

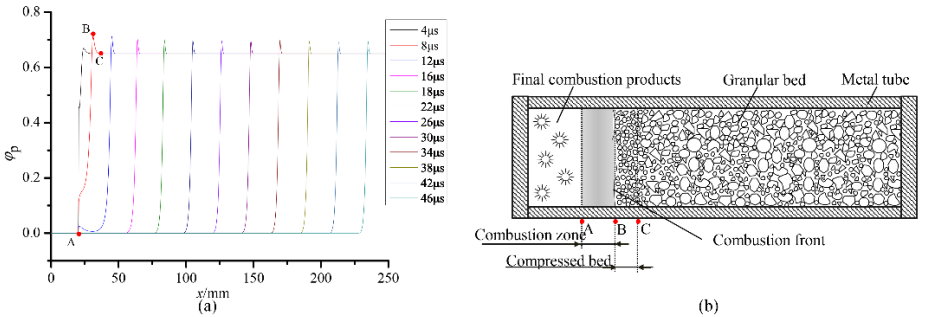

Figure 5. (a) Solid volume fraction evolution during the DDT process, (b) flame spreading and granular bed compression phenomena in a metal tube

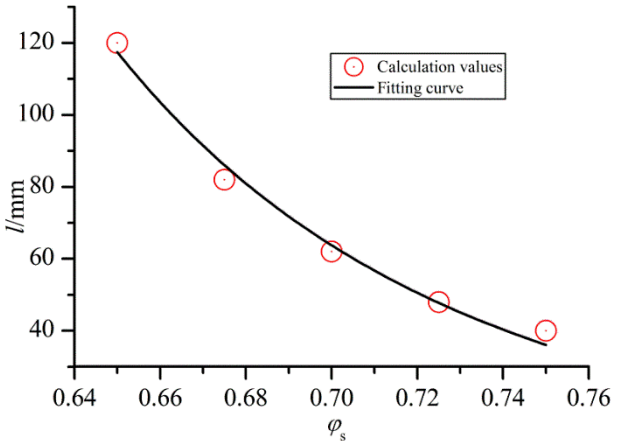

Figure 6. *l vs.* φ_s with a grain size of 200 μm

As is known, permeability is one of the important variables influencing DDT, which depends on convective heat transfer [24]. Furthermore there is a certain physical relationship between solid volume fraction and permeability. Thus, the solid volume fraction of energetic materials is one of the important parameters affecting run distance to detonation and time to detonation in a DDT process. In order to research the effect of solid volume fraction on DDT, the run distance to detonation with different solid volume fractions, such as 0.65, 0.675, 0.70, 0.725 and 0.75, was calculated. The relation of run distance to detonation (l) *versus* solid volume fraction (φ_s) is shown in Figure 6. The numerical results show that the run distance to detonation decreased as the solid volume fraction increased. That is because the solid volume fraction in the range $0.65 < \varphi_s < 0.75$, is low. With an increase in the solid volume fraction, the augmentation of energetic material in the unit volume, as well as the length of the flame area, decreased. That caused the release rate of gaseous products to be increased. Thereby, the run distance to detonation decreased. The fitting curve of l *vs.* φ_s is a semi-U type, which is reasonably consistent with that observed in experimental results [25, 26]. The results indicate that with an increase in the solid volume fraction, in the range $0.65 < \varphi_s < 0.75$, the tendency for DDT increased, and the safe performance of a high-energy solid propellant decreased.

3.3 Effect of pressure exponent on DDT

The pressure exponent n is an important index for the combustion performance of solid propellants and has a great influence on the pressure of the combustion process. In addition, the n value of a conventional solid propellant is generally equal to 0.4-0.6, but n is usually taken to be 1.0 during a simulated procedure, which conflicts with reality. Therefore, it was necessary to select a realistic pressure exponent to study the effects of n on the deflagration to detonation transition of propellants. In these calculations, the solid volume fraction φ_s was 0.73, and the grain size of the solid propellant was taken to be 200 μm. The pressure exponent n was selected in the range 0.4-0.7.

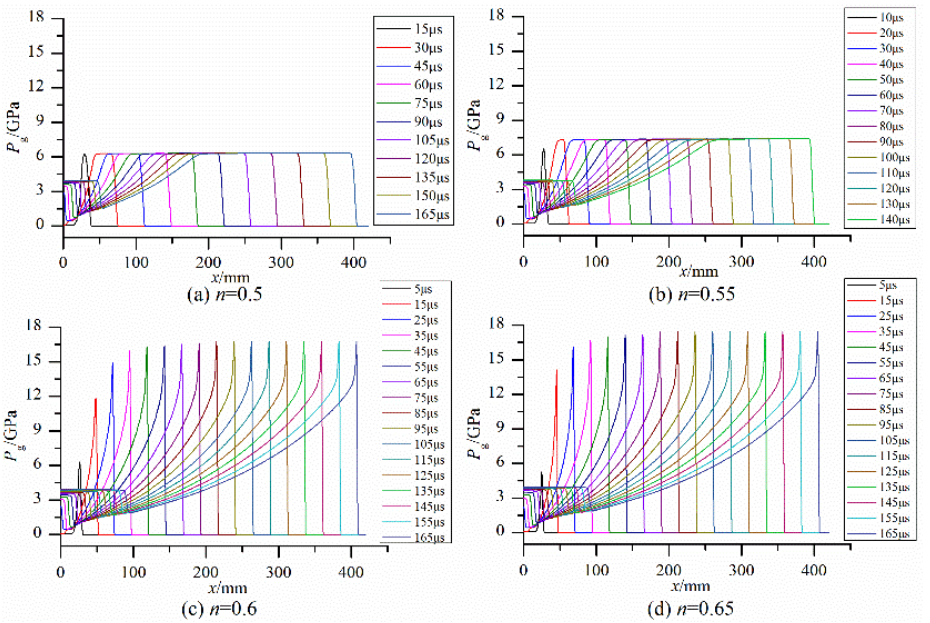

Figure 7. Gas pressure history profiles at different pressure exponents n

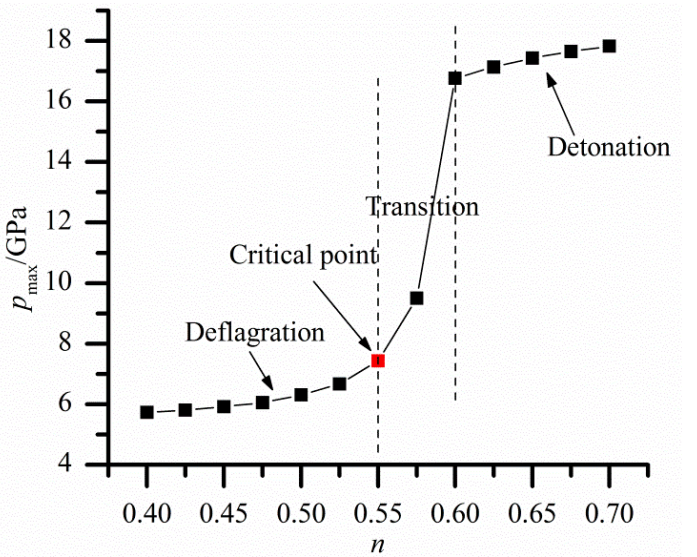

Figure 8. p_{max} *vs. n* with a grain size of 200 μm

Figure 7 shows the simulation results of gas pressure histories at different values of the pressure exponent *n*. It may be seen that the maximum gas pressure was 6.31 GPa and 7.42 GPa at $n = 0.5$ and 0.55, while the maximum gas pressure was 16.77 GPa and 17.43 GPa at $n = 0.6$ and 0.65. The maximum gas pressure was significantly increased from $n = 0.55$ to $n = 0.6$, but only a small increase from $n = 0.5$ to $n = 0.55$, as well as from $n = 0.6$ to $n = 0.65$. It is supposed that a critical transition occurs between 0.55 and 0.6. Figure 8 shows the variation in maximum gas pressure with the pressure exponent. The pressure exponent *n* plays an important role in the combustion process and the simulation results show that with an increase in *n*, the gas pressure and accelerating deflagration speed gradually increase. The gas pressure increased from 5.73 GPa at $n = 0.4$ to 6.31 GPa at $n = 0.55$. This is due to the increase of the pressure exponent *n* that leads to an increased burning rate of the solid propellant, and then leads to an acceleration of the gas release rate and the rise of gas pressure. When $n > 0.55$, a major new event was observed, the pressure rose rapidly, and detonation occurred when the pressure exponent was $n = 0.6$, where the detonation pressure reached 16.77 GPa. The detonation pressure increased slightly with a further increase in *n* for *n* greater than 0.6. In short, the pressure exponent *n* has a great influence on the pressure of the combustion stage, and $n = 0.55$ was the critical point for the deflagration to detonation transition of a solid propellant under the above conditions. But this has little influence on the pressure at a stable detonation stage.

4 Conclusions

In this study, a one-dimensional two-phase reactive flow model for the DDT process was constructed. A high resolution method, using a 5th-order WENO scheme for spatial discretization with a 3rd-order TVD Runge-Kutta method for time discretization, was applied to numerical calculations. Comparisons of the results presented for the inert two-phase shock tube problem showed good accuracy and convergence with numerical studies in the literature. The characteristics of a DDT process of a high-energy solid propellant were obtained and provided a better understanding of the effects of solid volume friction and pressure exponent on the DDT of a solid propellant.

It was found that for a solid propellant bed with a grain size of 200 μm and solid volume fraction of 0.65, the run distance to detonation was about 120 mm, the detonation induced time was 28 μs and the detonation pressure was about 18 GPa. The combustion process and the compression process were both observed in the deflagration stage as well as in the detonation stage. In both the deflagration and detonation stages, the thickness of the combustion zone is larger than the thickness of the compressed bed, and the two thicknesses in the detonation stage are smaller than those in the deflagration stage. In addition, an increase in the solid volume fraction caused the run distance to detonation and the safe performance of a high-energy solid propellant to decrease. The simulation results are in favorable agreement with experimental results.

The effects of the pressure exponent n on the deflagration to detonation transition were also discussed. The maximum gas pressure increased with the pressure exponent n, and $n = 0.55$ was a critical point for the deflagration to detonation transition of solid propellants.

References

[1] Macek, A. Transition from Deflagration to Detonation in Cast Explosives. *J. Chem. Phys*. **1959**, *31*(1), 162-167.

[2] Tarver, C.M.; Goodale, T.C.; Shaw, R.; Cowperthwaite, M. Deflagration-to-Detonation Transition Studies for Two Potential Isomeric Cast Primary Explosives. *Int. Det. Symp.*, *6th,* Coronado, **1976**, 231.

[3] Campbell, A.W. *Deflagration-to-Detonation in Granular HMX*. LANL Report LA-UR 80-2016, **1980**.

[4] McAfee, J.M.; Asay, B.W.; Bdzil, J.B. Deflagration to Detonation in Granular HMX. *Int. Det. Symp.*, *9th,* Portland, **1989**.

[5] McAfee, J.M.; Asay, B.W.; Bdzil, J.B. Deflagration-to-Detonation in Granular

HMX: Ignition, Kinetics, and Shock Formation. *Int. Det. Symp.*, *10th,* Boston, **1993**.
[6] Bernecker, R.R. The Deflagration-to-Detonation Transition Process for High-Energy Propellants – a Review. *AIAA J.* **1986**, *24*(1): 82-91.
[7] McAfee, J.M. The Deflagration-to-Detonation Transition. In: *Shock Wave Science and Technology Reference Library* (Asay, B.W., Ed.), Vol. 5, Springer, Heidelberg, **2010**, pp. 483-533; ISBN 978-3-540-87952-7.
[8] Stewart, D.S.; Asay, B.; Kuldeep, P. Simplified Modeling of Transition to Detonation in Porous Energetic Materials. *Phys. Fluids* **1994**, *6*: 2515-2534.
[9] Powers, J.M.; Stewart, D.S.; Krier, H. Analysis of Steady Compaction Waves in Porous Materials. *J. Appl. Mech*. **1989**, *56*(1): 15-24.
[10] Bdzil, J.B.; Son, S. *Deflagration-to-Detonation Transition*. LANL Report LA-12794-MS, **1994**.
[11] Asay, B.W.; Son, S.F.; Bdzil, J.B. The Role of Gas Permeation during Convective Burning of Granular Explosives. *Int J. Multiphase Flow* **1996**, *22*: 923-952.
[12] Baer, M.R.; Nunziato, J.W. A Two-phase Mixture Theory for the Deflagration-to-Detonation Transition (DDT) in Reactive Granular Materials. *Int. J. Multiphase Flow* **1986**, *12*(6): 861-889.
[13] Baer, M.R.; Gross, R.J.; Nunziato, J.W. An Experimental and Theoretical Study of Deflagration-to-Detonation Transition (DDT) in the Granular Explosive. *Combust. Flame* **1986**, *65*: 15-30.
[14] Powers, J.M.; Stewart, D. S.; Krier, H. Theory of Two-phase Detonation. Part I: Modeling. *Combust. Flame* **1990**, *80*(3): 264-279.
[15] Carroll, M.M.; Holt, A.C. Static and Dynamic Pore-Collapse Relations for Ductile Porous Materials. *J. Appl. Phys.* **1972**, *43*(4): 1626-1636.
[16] Butler, P.B.; Krier, H. Analysis of Deflagration to Detonation Transition in High-Energy Solid Propellants. *Combust. Flame* **1986**, *63*(1): 31-48.
[17] Narin, B.; Ozyoruk, Y.; Ulas, A. Two Dimensional Numerical Prediction of Deflagration-to-Detonation Transition in Porous Energetic Materials. *J. Hazard. Mater.* **2014**, *273*(3): 44-52.
[18] Dou, H.S.; Tsai, H.M.; Khoo, B.C.; Qiu, J. Simulations of Detonation Wave Propagation in Rectangular Ducts Using a Three-dimensional WENO Scheme. *Combust. Flame* **2008**, *154*(4):644-659.
[19] Dou, H.S.; Khoo, B.C. Effect of Initial Disturbance on the Detonation Front Structure. *Shock Waves* **2010**, *20*(2): 163-173.
[20] Sod, G.A. A Survey of Several Finite Difference Methods for Systems of Nonlinear Hyperbolic Conservation Laws. *J. Comput. Phys.* **1978**, *27*(1):1-31.
[21] Gonthier, K.A. Modeling and Analysis of Reactive Compaction for Granular Energetic Solids. *Combust. Sci. Technol.* **2003**, *175*(9): 1679-1709.
[22] Toro, E.F. *Riemann Solvers and Numerical Methods for Fluid Dynamics. A Practical Introduction.* Springer-Verlag, Berlin/Heidelberg, **2009**, pp. 151-162; ISBN 978-3-540-25202-3.
[23] Price, D.; Berneck, R.R. Deflagration to Detonation Transition of Porous Explosives. *High Dynamic Pressure*, *Proc., Symp.,* Paris, **1978**, 149-159.

[24] Keshavarz, M.H. A Simple Approach for Determining Detonation Velocity of High Explosive at Any Loading Density. *J. Hazard. Mater*. **2005**, *121*(1): 31-36.
[25] Obmenin, A.V.; Korotkov, A.I.; Sulimov, A.A.; Dubovitskii, V.F. Propagation of Predetonation Regimes in Porous Explosives. *Combust. Explos. Shock Waves* **1969**, *5*(4): 317-322.
[26] Saenz, J.A.; Stewart, D.S. Modeling Deflagration-to-Detonation Transition in Granular Explosive Pentaerythritol Tetranitrate. *J. Appl. Phys.* **2008**, *104*(4): 043519.

Received: September 4, 2018
Revised: December 12, 2019
First published online: December 20, 2019